Korean J. Chem. Eng., 33(10), 2771-2787 (2016)
DOI: 10.1007/s11814-016-0130-6
pISSN: 0256-1115
eISSN: 1975-7220

INVITED REVIEW PAPER

Stretchable carbon nanotube conductors and their applications

Sunju Hwang and Soo-Hwan Jeong†

Department of Chemical Engineering, Kyungpook National University (KNU), 80 Daehak-ro, Buk-gu, Daegu 41566, Korea
(*Received 8 March 2016 • accepted 5 May 2016*)

Abstract−Stretchable electronics has evolved rapidly in the past decade because of its promising applications, as electronic devices undergo large mechanical deformation (e.g., bending, folding, twisting, and stretching). Stretchable conductors are particularly crucial for the realization of stretchable electronic devices. Therefore, tremendous efforts have been dedicated toward developing stretchable conductors, with a focus on conductive material/polymer composites. This review summarizes the recent progress in stretchable conductors and related stretchable devices based on carbon nanotubes (CNTs), which was enabled by their outstanding electrical and mechanical properties. Various strategies for developing highly stretchable conductors that can deform into nonplanar shapes without significant degradation in their electronic performance are described in terms of preparation processes. Finally, challenges and perspectives for further advances in CNT-based stretchable conductors are discussed.

Keywords: Carbon Nanotube, Stretchable Conductors, Nanomaterials, Strain Sensors, Supercapacitors

INTRODUCTION

The field of electronics is rapidly evolving beyond conventional rigid electronics based on Si materials toward a new paradigm of stretchable electronics, where electronic devices can be deformed in various ways. In the past decade, rapid developments in stretchable electronics have imparted mechanical flexibility and stretchability to otherwise rigid and brittle electronic devices based on Si wafers, introducing novel applications in wearable computers, artificial skins, health monitoring devices, smart clothes, etc. [1-6]. Various stretchable devices have been successfully developed, including stretchable conductors, light-emitting diodes (LEDs), batteries, displays, and sensors [7-12]. In these devices, stretchable conductors are basic and indispensable components of the stretchable electronic systems because they not only serve as electrodes but also interconnect to other components.

A common strategy to obtain stretchable conductors is depositing nanomaterials on or embedding them inside elastomers to form composites. The conductive materials can be a conducting polymer such as poly(3,4-ethylenedioxythiophene) : poly(styrenesulfonate) (PEDOT : PSS) [13,14], metal nanomaterials [15-17], graphene [18,19], or carbon nanotubes (CNTs) [20-27]. These materials offer good electrical conductivity, and the elastomers provide mechanical deformability and protect the rigid conductive materials from fracture under stretching. Among them, CNTs have great promise for high-performance stretchable electronics owing to their outstanding mechanical flexibility, electrical property of a high carrier mobility, and chemical stability [28-30]. Although a few outstanding review articles regarding stretchable electronics [31-34] including metal nanowire-based stretchable conductors have been published [35], a state-of-the-art review with a focus on the stretchable conductor based on CNTs has never appeared.

In this review, we focus on CNT-based stretchable conductors, along with their applications. In Section 2, we summarize the recent advances in the fabrication methods of stretchable conductors using CNTs. In Section 3, we summarize the representative applications of these stretchable conductors. Finally, we discuss challenges and future directions for CNT-based stretchable conductors and related devices.

CNT-BASED STRETCHABLE CONDUCTORS

CNTs are composed of either one rolled graphite sheet (single-walled CNT (SWCNT)) or multiple rolled graphite sheets (multi-walled CNT (MWCNT)) in a cylindrical tube shape [36]. One-dimensional (1D) CNTs with a high aspect ratio exhibit outstanding properties, such as mechanical robustness, high thermal stability, and good electrical conductivity [37,38]. For example, CNTs have an extremely high aspect ratio exceeding 10^6, a Young's modulus of ~1 TPa, a tensile strength of ~100 GPa, and a current-carrying capacity of 10^9 A cm^{-2}. These superior properties make CNTs fascinating nanomaterials for stretchable conductors. CNT-based conductors can be categorized into four types according to the preparation process: i) CNT/polymer mixtures, ii) solution-processed CNT film/polymer composites, iii) dry-processed CNT film/polymer composites, and iv) CNT yarn/polymer composites.

1. CNT/Polymer Mixtures

At an early stage of development for the fabrication of CNT-based stretchable conductors, CNT/polymer mixtures were widely studied. These mixtures were obtained by the direct dispersion of CNTs within the polymer matrix or the infiltration of CNTs in a soft polymer such as polydimethylsiloxane (PDMS) or polyurethane (PU). In such cases, CNTs easily form a network configuration in the CNT/polymer composite, serving as a conductive passage and can

†To whom correspondence should be addressed.
E-mail: shjeong@knu.ac.kr

accommodate tensile strain by sliding against each other when a tensile strain is applied.

One approach for preparing CNT-enabled stretchable conductors is to disperse CNTs into elastomeric materials. For instance, uniformly dispersed SWCNT composite films were developed by blending millimeter-long SWCNTs, an ionic liquid, and a fluorinated copolymer matrix, as presented in Fig. 1(a) [27]. While the SWCNT composite exhibited a high electrical conductivity of 57 S cm^{-1}, it was uniaxially stretched by only 38%. To improve the elasticity of the SWCNT composite, it was perforated with a net-shape structure using a mechanical punching system and then coated with PDMS. The resultant conductor exhibited an enhanced uniaxial stretchability of 134% with the same initial conductivity as the composite. Although the conductivity decreased to 6 S cm^{-1} when the conductor was stretched to 134%, this value exceeded the conductivity of the commercial conducting rubber (0.1 S cm^{-1}). Using this approach, Shang et al. [39] developed stretchable conductors by the sonication of pretreated MWCNTs, ionic liquid, and a PU solution. After the dispersion step, the fabricated composite was stretched and released ten times at 100 °C to align the MWCNTs within the polymer matrix. The MWCNT/PU composites exhibited no significant degradation of conductivity after 100 stretching/releasing cycles for a tensile strain up to 100%, indicating their excellent durability. This result suggested that repeated stretching/releasing can yield a higher degree of alignment and a stabilized structure without damaging the conductive network. The CNTs slid against each other and were rearranged under the tensile strains, and during the releasing process the conductive network was restored to its original state.

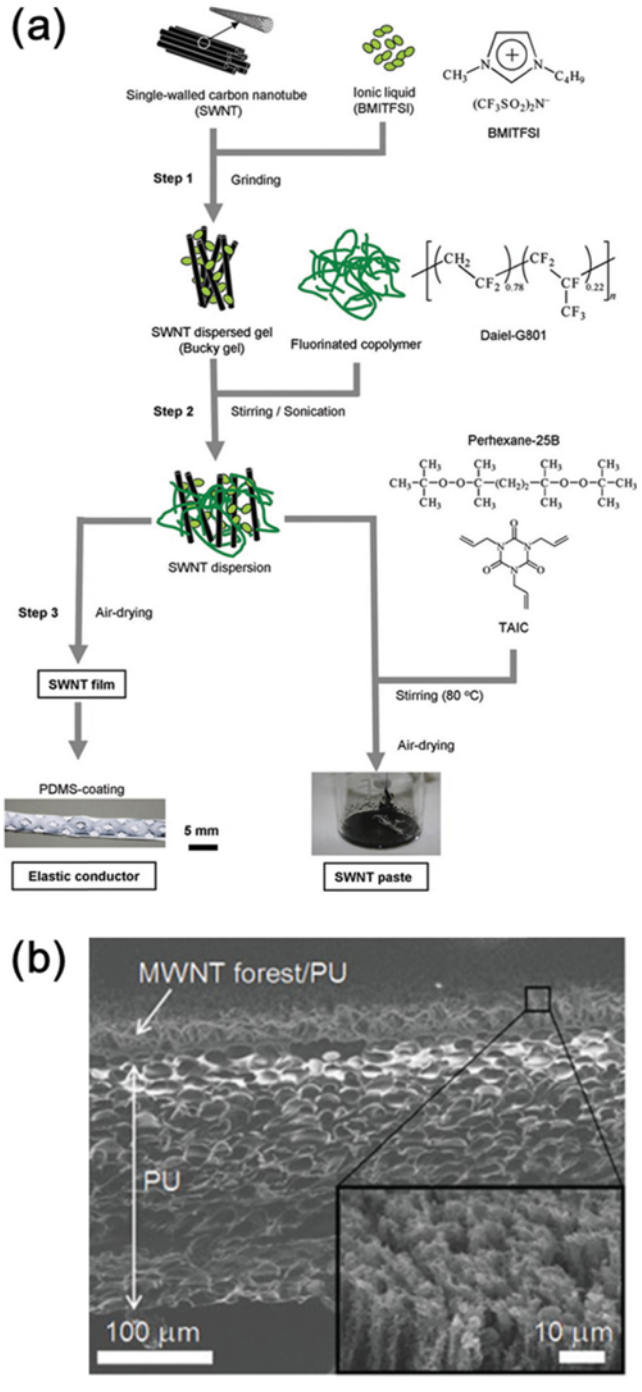

Fig. 1. (a) Fabrication process for SWCNT film, SWCNT elastic conductor, and SWCNT paste. Reproduced from Ref. [41] with permission (Copyright 2008, The American Association for the Advancement of Science). (b) SEM image of the MWCNT forest/PU composite sheet cross section. The inset shows a high-magnification image of the black forest side. Reproduced from Ref. [42] with permission (Copyright 2010, Wiley).

Unlike previously developed stretchable conductors, which contain a large amount of CNTs (>10 wt%), SWCNT/silicone rubber composites were prepared by mixing ionic liquid and silicone rubber with an SWCNT content of only 4 wt% [40]. Although the high loading of CNTs into the polymer is necessary to achieve a high conductivity, it generally results in increased stiffness and poor stretchability of the composite [41-43]. To solve this dilemma, nitric-acid doping was performed to achieve a high conductivity at a moderately low CNT content without losing the elasticity of the composites. CNTs are very sensitive to chemical doping [44], and acid treatments have proven to be an effective doping method for improving their electrical conductivity. This redox dopant introduces hole doping into the CNT network and lowers the Fermi level [45]. The composites exhibited a low sheet resistance of 50 Ω sq^{-1} (63 S cm^{-1}) after the nitric-acid treatment. Even after 20 stretching/releasing cycles for a tensile strain up to 200%, the conductivity remained at 18 S cm^{-1}.

In the aforementioned approach, the uniform dispersion of CNTs within the polymer is crucial for obtaining highly stretchable conductive composites. Owing to the van der Waals attraction forces between CNTs, CNTs tend to agglomerate during dispersion, yielding a low electrical conductivity. Many techniques, such as ultrasonication [40,46], jet-milling [7], high-shear processing [47,48], and exfoliation agents (e.g., ionic liquids) [7,39,40], have been introduced to ensure the homogeneous dispersion of CNTs.

On the other hand, the infiltration method does not require the dispersion of CNTs in the polymer. For example, Shin et al. [42] fabricated rubber-like MWCNT forest/PU composites by using this infiltration strategy. CNT forests are three-dimensional (3D) structures composed of vertically aligned arrays of CNTs that can be grown by chemical vapor deposition (CVD). The grown MWCNT forests were infiltrated with a PU solution, producing effective bond-

Table 1. Summary of the performance of stretchable conductors based on CNTs

Materials	Strategy	Transmittance	Initial electrical property	Electrical property under tensile strain	Durability (cyclic test)	Applications	Ref.
SWCNTs/ fluorinated copolymer matrix	Mixture	-	σ^a: 57 S cm^{-1}	σ: Stable at 57 S cm^{-1} within ε^b=40%, decrease to 6 S cm^{-1} within ε=134%	σ: Stable for 4,000 cycles (ε_{max}=25%)	Organic transistors	[41]
MWCNTs/ PU matrix	Mixture	-	σ: 5.3 S cm^{-1}	σ: Stable within ε=100%	σ: Almost stable for 100 cycles (ε_{max}=100%)	-	[39]
SWCNTs/ silicone rubber	Mixture	-	R_s^c: 50 Ω sq^{-1} (σ: 63 S cm^{-1})	R_s: 320 Ω sq^{-1} (σ: 19 S cm^{-1}) at ε=300%	σ: 18 S cm^{-1} after 200 cycles (ε_{max}=200%)	-	[40]
MWCNT forests/PU	Mixture	-	σ: 0.5-1 S cm^{-1}	R: Increase by ~10% at ε=30%	R: Almost stable for 100 cycles (ε_{max}=40%), except for the initial increase	-	[42]
SWCNT aerogels/ PDMS	Mixture	~93%	σ: 1.08 S cm^{-1}	R: Increase by ~14% at ε=100%	R: Almost stable for 20 cycles (ε_{max}=100%)	-	[49]
SWCNT films/ PtBA	Bar-coating	~87%	R_s: 500 Ω sq^{-1}	R: Almost constant within ε=10%, linearly increase by 50% within ε=50%	-	Polymer light-emitting electrochemical cells	[24]
		~77%	R_s: 200 Ω sq^{-1}	R: Increase by 78% within ε=50%	R: Increase by 14% after 14 cycles (ε_{max}=40%)		
SWCNT films/ PDMS	Spray-coating	~68%	σ: 1,100 S cm^{-1} for 100 nm film	σ: 2,200 S cm^{-1} at ε=150%	R: Increase by 10% after 4 cycles (ε_{max}=50%)	Strain and pressure sensors	[22]
SWCNT films/ PDMS	Spray-coating	65% for 1 time of spray <20% for 3 times of spray	R: ~12 kΩ R: 564 Ω	R: Increase to 789 Ω at ε=50%	R: Almost stable for 100 cycles (ε_{max}=50%), except for first cycle	LEDs, touch pads, strain and pressure sensors	[51]
CNT nanomesh films/PDMS	Layer-by-layer deposition, cross-stacked	78%	R_s: 264 Ω sq^{-1}	R: Increase by 35% at ε=30% (diagonal stretching)	R: Almost stable for 500 cycles (ε_{max}=30%, diagonal stretching)	LEDs	[56]
CNT films/ PDMS	Ink-jet printing	58.3% for 1-layer -	R_s: 196.76 Ω sq^{-1} R_s: 19.08 Ω sq^{-1} for 5-layer	R: Slightly increase within ε=100%	- R: Increase by 20% after 1,000 cycles (ε_{max}=100%)	LEDs	[58]
SWCNT films/ PDMS	CVD	62%	R_s: 53 Ω sq^{-1}	R: Increase by 5% within ε=10%	R: Stable for 500 cycles (ε_{max}=40%), except for the initial increase	LEDs	[62]

Table 1. Continued

Materials	Strategy	Transmittance	Initial electrical property	Electrical property under tensile strain	Durability (cyclic test)	Applications	Ref.
SWCNT films/ PDMS	CVD, prestrain	-	-	R: Almost stable within ε=140%	-	LEDs, supercapacitors	[110]
Aligned CNT films/PDMS	Drawing, prestrain	~60%	R: 18.8 kΩ	R: Increase by 1.5 times within ε=120%	R: Almost stable after 6 cycles (ε_{max}=100%)	-	[21]
Aligned CNT films/PDMS	Drawing, prestrain	-	R: 610 Ω	R: Increase by 4.1% within ε=100% (prestrain level)	-	LEDs	[70]
Aligned CNT films/PDMS	Prestrain	-	R_s: ~650 Ω sq^{-1}	R: Increase by 6% within ε=100% (prestrain level)	R: Almost stable for 30 cycles (ε_{max}=100%)	-	[71]
Aligned CNT films/PDMS	Cross-stacked	39% for 4-layer	R_s: ~405 Ω sq^{-1}	R: Increase by 15% at ε=28%	R: Almost stable after 200 cycles (ε_{max}=15%)	-	[23]
Aligned CNT films/PDMS	Drawing, prestrain, cross-stacked	-	R: 430 Ω for parallel	R: Increase by 4.1% at ε=200% (prestrain level)	R: Increase by <5% after 10,000 cycles (ε_{max}=150%)	LEDs	[72]
			R: 497 Ω for cross-stacked	R: Increase by 1.7% at ε=40% (prestrain level)	R: Increase by <7.5% after 10,000 cycles (ε_{max}=40%)		
CNT yarns/ PDMS	Spinning, prestrain	-	R: ~2.6 kΩ	R: Increase by only 1% at ε=40% (prestrain level)	R: Almost stable for 20 cycles (ε_{max}=40%)	-	[89]
CNT yarns/ PDMS	Spinning, prestrain	-	R: 5,500 Ω for the buckled dry spun CNT yarn	R: Almost stable within ε=40% (prestrain level)	R: Increase by ~0.2% after 10,000 cycles (ε_{max}=40%)	Supercapacitors	[88]
CNT yarns	Spinning, twisting	-	σ: 440 S cm^{-1}	R: Increase by <2% within ε=20%	R: Almost stable for 1,000 cycles (ε_{max}=20%)	-	[90]
CNT yarns	Spinning, twisting	-	R: ~10.88 Ω	R: Increase by ~3.2% within ε=25%	R: Almost stable for 1,000 cycles (ε_{max}=25%)	-	[81]

[a]Conductivity
[b]Applied tensile strain
[c]Sheet resistance

ing between the PU and the nanotubes with highly porous foam, as shown in Fig. 1(b). The resultant composites exhibited a superb stretchability over 1,400%, negligible resistance change during 100 bending and twisting cycles, and highly reversible changes in resistance within a moderate strain range (up to 20%). These features indicate that the 3D structure of the conductive CNT network held together with the elastic polymer binder retained its original shape upon stretching. A similar but modified approach was also demonstrated. Kim et al. [49] fabricated stretchable conductors by backfilling SWCNT aerogels, which are highly porous 3D networks of SWCNTs, with the elastomer PDMS. In this study, a transparent SWCNT aerogel/PDMS composite film with a transmittance of ~93% was obtained. The initial conductivity of the transparent film (0.83 S cm^{-1}) was slightly lower than that of the non-transparent one (1.08 S cm^{-1}). Both composite films exhibited a nearly constant resistance after 20 stretching/releasing cycles for a maximum tensile strain of 100%. Upon stretching, the 3D networks of SWCNTs produced sliding between the nanotubes without losing contact, supported by the PDMS.

Although CNT/polymer mixture composites can be obtained by a relatively simple process, they are usually opaque owing to the high loading of CNTs. To broaden the applications of stretchable conductors, especially in the field of optoelectronics, imparting optical transparency to stretchable conductors is necessary. Therefore, extensive efforts have recently been directed toward developing transparent and stretchable conductors based on CNTs, i.e., forming CNT film/polymer composites.

The overall performance of stretchable conductors based on CNTs is summarized in Table 1.

2. Solution-processed CNT Film/Polymer Composites

In addition to CNT/polymer mixtures, CNT film/polymer composites can be fabricated to achieve stretchability. CNTs can be formed into thin films by solution-based coating methods (e.g., spray- [22,50,51], dip- [52-54], spin- [55], and bar-coating [24]), which yield randomly distributed CNTs. The randomly oriented CNT films may have an improved optical transparency compared with CNT/polymer mixtures, which are generally filled with a relatively large amount of CNTs.

As an example of solution-processed CNT film-based conductors, Yu et al. [24] prepared a SWCNT film/polymer composite by bar-coating a SWCNT dispersion with a Meyer rod on a glass, conducting polymerization, and peeling the film off of the glass. The composite had a sheet resistance of 500 Ω sq^{-1} and a high transparency; the transmittance was ~87% at a wavelength of 550 nm. The resistance of the composite was almost constant below a tensile strain of 10% and then linearly increased by over 50% for a tensile strain up to 50%.

On the other hand, Lipomi et al. [22] spray-coated a CNT solution directly onto a PDMS substrate to fabricate stretchable and transparent CNT-based conductors. The transmittance of the spray-coated CNT film was ~79%. By applying a tensile strain along both horizontal and vertical axes, the CNT film was rendered reversibly stretchable in any direction. As shown in Fig. 2(a), this biaxial stretching and releasing process induced a buckling configuration of all the CNT bundles. The resultant conductors endured tensile strains as large as 150%, with a high conductivity of 2,200 S cm^{-1}.

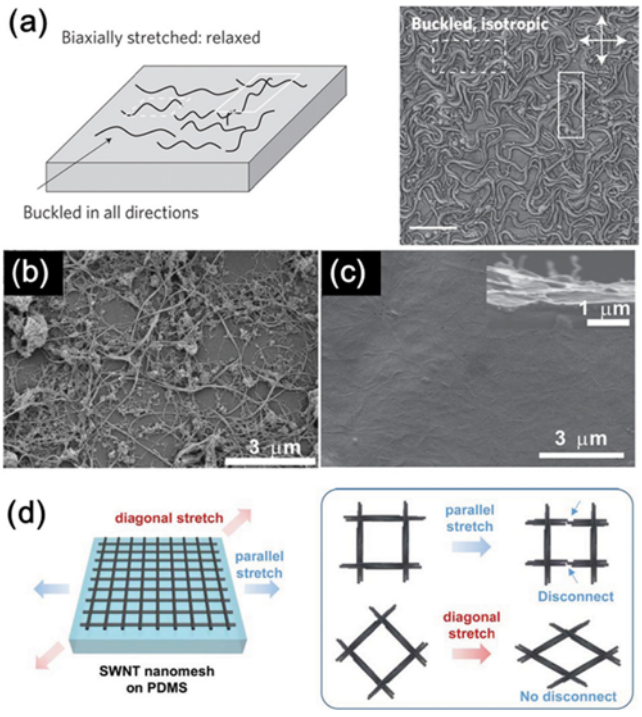

Fig. 2. (a) Schematic (left) and corresponding AFM phase image (right) of CNT/PDMS film being stretched and released along two axes. The dashed and solid white boxes show the CNT bundles buckled along the horizontal and vertical axes, respectively. Scale bar: 600 nm. Reproduced from Ref. [22] with permission (Copyright 2011, Nature Publishing Group). (b), (c) SEM images of the SWCNT/PDMS film on the glass slide (b) and after being buried to just below the PDMS surface (c). The inset shows a cross-sectional SEM image. (b), (c) Reproduced from Ref. [51] with permission (Copyright 2013, Royal Society of Chemistry). (d) Schematic showing the stretching of SWCNT nanomesh films on PDMS in the parallel and diagonal directions. Reproduced from Ref. [56] with permission (Copyright 2015, Royal Society of Chemistry).

In the aforementioned stretchable conductors with the spray-coated CNT film, the CNTs were deposited on top of elastomers. To prevent the CNTs from delamination or peeling off and enhance the mechanical stability of the spray-coated CNT film-based conductors, Wang et al. [51] coated a fluorinated substrate with a CNT suspension and transferred the CNT film onto PDMS. The transmittance was as high as 65% at a wavelength of 550 nm, and the initial sheet resistance was as low as 564 Ω sq^{-1}. Compared with the SWCNT film coated on the glass slide (Fig. 2(b)), most of the SWCNTs were buried below the surface of PDMS; only a few CNTs were on the surface (Fig. 2(c)). Thus, only a few nanotubes were peeled off by the first tape test, and the conductor retained its conductivity even after 10 tape tests. During 100 stretching/releasing cycles for a strain of 50%, the resistance of the conductor retraced itself and decreased under the strain after the first cycle, without any cracks, de-bonding, or peeling between the nanotubes and PDMS. These results indicate that the CNTs buried below the surface of the elastomers provided the conductors with excellent mechanical stability.

To obtain highly conductive and transparent CNT conductors, it is important to form well-connected conducting paths with relatively low CNT concentrations. For this purpose, electrospun polymer nanofibers have been introduced as template to assist in the deposition of CNTs at desired locations for producing a continuously connected conducting network of CNTs without agglomeration [52-54]. Kim et al. [54] employed electrospun PU nanofibers with a web structure (nanoweb) as a stretchable scaffold for CNT deposition because of the attractive interactions of PU with CNTs and the inherently elastic characteristics of PU. A stretchable and transparent CNT conductor, which had a sheet resistance of 424 Ω sq^{-1} at 63% transmittance, was developed by dipping the PU nanoweb into an acid-treated SWCNT solution and washing in distilled water nine times, followed by chemical doping. When the dipping and doping processes were performed using a prestrained elastomer, a noodle-like and buckled morphology was obtained. The prestrained conductors accommodated a tensile strain of 100% with an increase in resistance of only ~1.3, which was far less than that of the pristine conductor (4.4). After only six stretching/releasing cycles for a tensile strain up to 100%, the resistance was nearly stable. This negligible change in resistance was attributed to the straightening of the buckled PU fibers under tensile strains.

Although the aforementioned solution-based coating methods mostly produced random networks of CNTs, CNT films with a non-random mesh structure were obtained via the template-guided self-assembly of CNTs [56]. This process started with attaching a square-shaped PDMS frame to the glass. Then, the SWCNT solution was coated onto the glass substrate and covered with the nano-patterned PDMS mold. After a vacuum was applied, the SWCNT solution was confined between a nano-patterned mold and a substrate. During the evaporation of the solution, the confinement of the SWCNTs produced aligned CNTs arrays, which were parallel to the lines on the PDMS mold. Lastly, SWCNT nanomesh films were fabricated by repeating the aforementioned procedures in the transverse direction to the previous aligned CNTs patterns. The resultant SWCNT nanomesh films exhibited a sheet resistance of 264 Ω sq^{-1} with a transmittance of 78%. The relative resistance change $\Delta R(=R-R_0)/R_0$—where R and R_0 are the electrical resistances in the strain and relaxed states, respectively, of the SWCNT nanomesh films—was 0.35 at a tensile strain of 30% under diagonal stretching, which was 7.7 times lower than that of the random network (2.69). The nanomesh films exhibited ~42 times less resistance increase after 500 stretching/releasing cycles at a strain of 30%. This enhanced stretchability and mechanical durability were attributed to the deformation of the mesh structure during the diagonal stretching; the square shape was deformed into a rhombus without the breakage of nanotubes, as displayed in Fig. 2(d). On the other hand, the random network may fracture under large tensile strains because of the stress concentration at the weakly bonded nanotubes.

In addition to coating methods, the inkjet printing method is a viable process for producing stretchable CNT conductors. It is promising owing to its low fabrication costs and large-area scalability, which enable direct patterning without an expensive and sophisticated lithography process [57]. By inkjet-printing an aqueous SWCNT ink on a PDMS substrate, Kim et al. [58] successfully fabricated high-performance stretchable conductors wherein the sheet resistances of 1- and 5-layer printed SWCNT films were 169.76 and 19.08 Ω sq^{-1}, respectively. A durability test on 5-layer printed samples exhibited an increase of less than 20% in the resistance after 1,000 stretching/releasing cycles under a tensile strain of 100%. An alternative approach based on a solution method

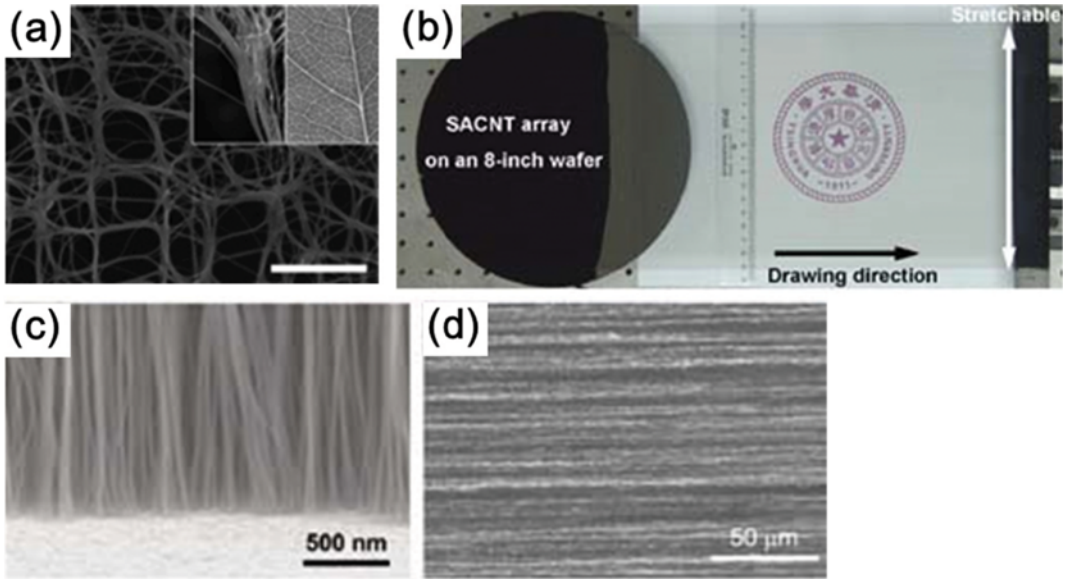

Fig. 3. (a) SEM image of the as-grown SWCNT film with a hierarchical reticulate structure. Scale bar: 500 nm. The insets compare the reticulate structure of the SWCNT film (left) and the leaf veins (right). Reproduced from Ref. [62] with permission (Copyright 2012, Wiley). (b)-(d) Super-aligned CNT film: (b) a transparent CNT film drawn out of a super-aligned CNT forest on an 8-inch silicon wafer. (c), (d) SEM images of the super-aligned forest on the silicon wafer from a side view (c) and the super-aligned CNT film from a top view (d). (b)-(d) Reproduced from Ref. [68] with permission (Copyright 2010, Wiley).

involves vacuum filtering a CNT solution over a porous filtration membrane and then peeling the collected CNT film off of the membrane. This method can yield a uniform film and easily control the thickness of the filtrated CNT films according to the concentration and volume of the CNT solutions [59]. Relying on vacuum filtration of CNT dispersion and the transfer of the resultant CNT films onto the silicone, Cohen et al. [60] obtained elastic CNT film composites that could be stretched by a tensile strain of 100%.

3. Dry-processed CNT Film/Polymer Composites

Another approach for producing CNT films is called dry-processing because it does not require a CNT solution. It involves direct floating-catalyst CVD growth and then drawing out from super-aligned and vertically grown CNT forests. In the former method, methane and ferrocene/sulfur powder are used as carbon and catalyst sources, respectively. At a high reaction temperature (1,050-1,100 °C), the bundles in the films densely connect with each other when they are growing to form a continuous two-dimensional network. Consequently, the directly synthesized CNT film exhibits a unique hierarchical reticulate structure, which is similar to the veins of leaves, as shown in Fig. 3(a). Because of the 1-μm-long interconnected bundles in the resultant film, the film has excellent electrical and mechanical properties compared with CNT films obtained via solution-based filtration: the electrical conductivity and mechanical strength are 2,000 S cm^{-1} and 360 MPa, respectively [61]. By embedding the directly grown CNT films with the reticulate structure into PDMS, Cai et al. [62] reported highly transparent and conductive stretchable conductors, which had a transmittance ranging from 62 to 16% at a wavelength of 550 nm and a sheet resistance ranging from 53 to 7 Ω sq^{-1}. Under cyclic strain tests with 40% strain for 500 cycles, the resistance remained unchanged, except for a rapid increase in the initial cycles. However, the conductors became fractured at a strain of 60% with a resistance increase of 125%.

Unlike the direct CVD growth strategy, the latter method involves a conversion from a super-aligned CNT forest to a thin film, as previously mentioned. The super-aligned CNT forests are distinguished from ordinary vertically aligned CNT forests by their high degree of alignment, which is caused by the high nucleation density and narrow diameter distribution as well as their very clean surfaces. The clean surfaces of CNTs lead to strong van der Waals interactions between the CNTs, enabling them to be connected end-to-end and drawn into continuous films [63-65]. By using tweezers to pull out or a blade to scratch off CNT bundles from the forests, a continuous super-aligned CNT film can easily be obtained. The drawing process is presented in Fig. 3(b), and the super-aligned CNT forest and super-aligned CNT film drawn out of the forest are shown in Figs. 3(c) and (d), respectively. The as-drawn CNT films are ultrathin, lightweight, and transparent, and they exhibit excellent mechanical strength along their drawing direction because the alignment of the CNTs is nearly parallel to the drawing direction [65-68]. The other feature of the drawing approach is the total conversion of CNT forest into the films without wasting CNTs. This differs from the solution-based process, which typically causes a serious loss of CNTs. In the solution approach, commercial CNT powder is dispersed in the solvents before coating onto the substrate. Abundant conglomerations may be observed in the dispersion step owing to their entanglement during industrial CVD growth; accordingly, only a small amount of CNTs is utilized to fabricate films [68]. The aforementioned advantages of the drawn CNT films motivated tremendous research efforts regarding the development of stretchable conductors based on drawn CNT films. For example, Zhang et al. [21] fabricated a stretchable conductor by embedding a drawn CNT film within the PDMS. The resulting conductor exhibited a transparency of ~60% in the wavelength range of 400 to 800 nm. In the first stretching process, the CNTs slid against each other along the tensile direction, and the connection became weak, increasing in resistance. When the conductor was released, the connections between the CNTs were improved, and uniform buckled structures were formed. Upon the second stretching, the buckled structures accommodated the tensile strain by straightening, without an obvious resistance change. The following stretching/releasing cycles improved the CNT arrangement, and a stable resistance (35.5±0.3 kΩ, standard deviation: 0.8%) was achieved after six cycles of 100% stretching, indicating great reversibility. This electrical performance under cyclic tests with a tensile strain demonstrated that the buckled shape rendered the conductor more stretchable without a loss of electrical conductivity during the stretching. The same trend of buckled CNTs is observed in another report [69]. To understand how the buckles formed, the morphology changes of four neighboring CNTs on a PDMS substrate were investigated using an optical microscope as the substrate was stretched and released. The deformation of CNTs under different strain levels is depicted in Fig. 4(a). Under tensile strains (i-iii), the CNTs slid against each other, reducing the overall contact area between the CNTs. This is why the resistance of the CNT-film conductors increased under the first stretching. During the release (iv, v), the CNTs buckled and did not slide back. The electric response of a buckled CNT on PDMS was also observed at different compressive and tensile strains. As shown in Fig. 4(b), the resistance remained almost constant under compressive and tensile strains. This result is related to the reason why the CNT film-based conductor exhibited a stable resistance after the second stretching/releasing.

Similarly to the formation of the buckled configuration by repetitive stretching/releasing cycles, CNT films can be transferred onto a prestrained elastomeric substrate to generate a periodic buckled geometry after releasing the prestrained substrate. This prestrain approach is simple and straightforward. Because the wavelength and amplitude of curved CNTs increase and decrease, respectively, according to the level of stretching, buckled CNT conductors outperform stretchable conductors comprising straight CNTs and exhibit a nearly negligible resistance change with a tensile strain up to the prestrain level. Using the prestrain strategy, Xu et al. [70] fabricated stretchable conductors based on buckled CNT films. Releasing the prestrained PDMS substrate produced a periodic out-of-plane buckling of the CNT films, as shown in Fig. 4(c). The buckled CNT films were coated with a thin PDMS layer to protect them from contamination. The initial resistance of the conductor was 610 Ω In the out-of-plane buckled morphology, CNT sliding occurred only in the flat region, which was in contact with the substrate. Thus, the resistance increased by only ~4.1%, to the

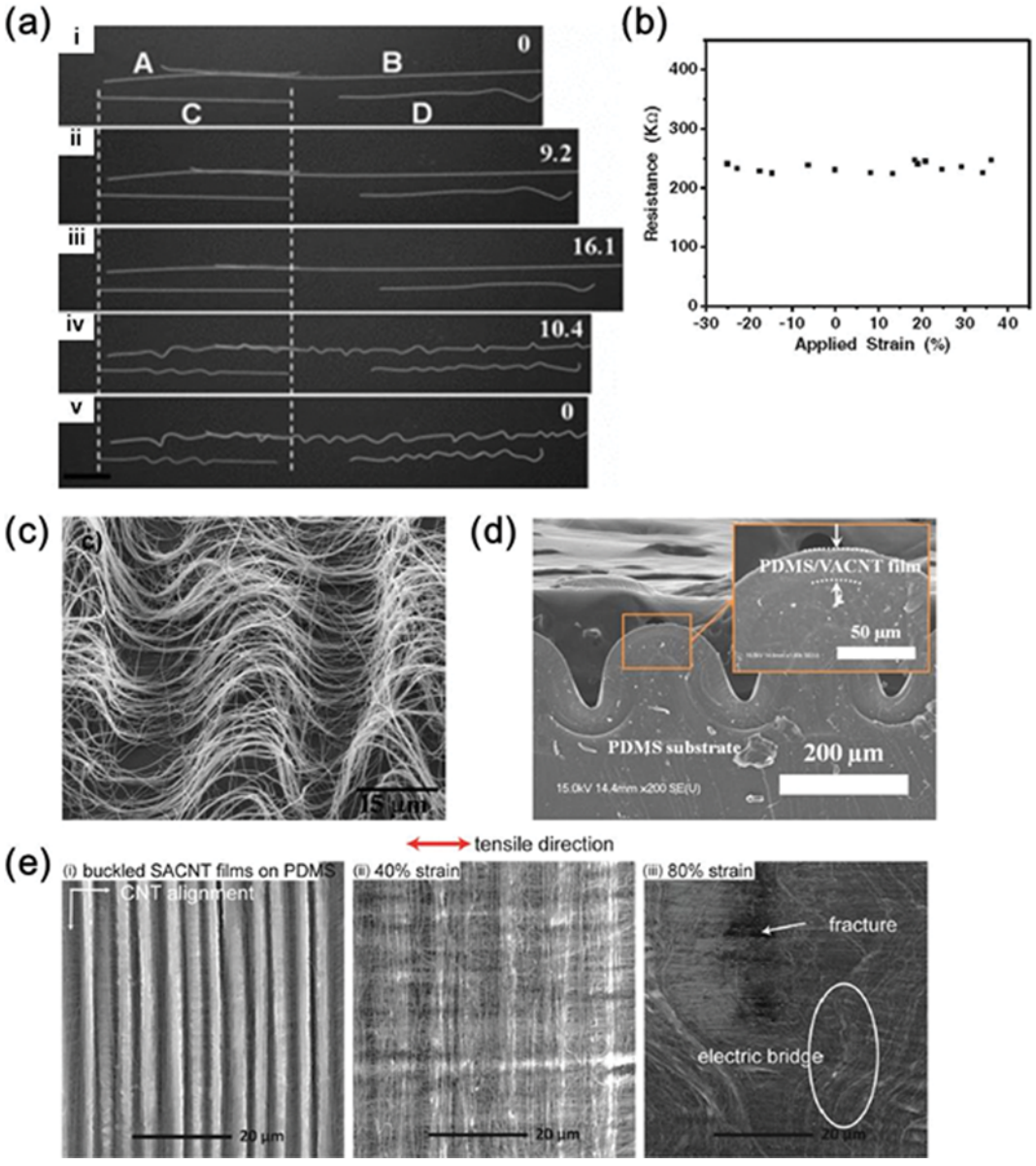

Fig. 4. (a) Optical images of four CNTs (labeled A, B, C, and D) under different strain levels (indicated on the right in percentage) during stretching (i-iii) and releasing (iv, v) process. Scale bar: 10 μm. (b) The resistance of the buckled CNT on PDMS at different compressive and tensile strains. (a), (b) Reproduced from Ref. [69] with permission (Copyright 2012, Wiley). (c) SEM image of a buckled CNT film after the release of the prestrained PDMS. The image was taken by tilting the sample at an angle of 20°. Reproduced from Ref. [70] with permission (Copyright 2012, Wiley). (d) Cross-sectional SEM image of a wavy PDMS-embedded vertically aligned CNT film on a PDMS substrate. The inset shows a magnified SEM image of the film. Reprinted from Ref. [71] with permission (Copyright 2014, American Chemical Society). (e) *In situ* SEM images of wavy cross-stacked super-aligned CNT films on PDMS and the morphology evolution at applied strains of 40% and 80%. Reproduced from Ref. [72] with permission (Copyright 2015, Royal Society of Chemistry).

prestrain value (100%). However, when the applied strain exceeded the prestrain, all of the straightened CNTs slid against each other, causing a rapid resistance increase. To improve the conductivity, the aligned CNT films were coated with a thin film of an Au/Pd alloy. Similarly, using the prestrain method, buckled stretchable conductors based on PDMS-infiltrated CNT films were fabricated [71]. Prior to transferring the PDMS-infiltrated CNT film, thin liquid PDMS was spin-coated onto the prestrained PDMS to improve the interaction between the films and substrate and enhance the mechanical robustness. Fig. 4(d) suggests that the PDMS-infiltrated CNT film was well-established on top of the PDMS, with periodic buckled patterns. The resultant conductor exhibited small resistance changes less than 6% for a tensile strain up to 100% (prestrain level) and a stable resistance change under 30 stretching/releasing cycles with a maximum strain of 100%. This cyclic test revealed that the crack-free structure of the PDMS-infiltrated CNT film and its excellent adhesion to the substrates played an important role in the stability of the conductors under mechanical defor-

mations.

However, super-aligned CNT films have an anisotropic electrical property (e.g., the ratio of the sheet resistances in the perpendicular direction to those in the parallel direction was ~100 : 1 [23]) because of the unidirectional drawing process. This anisotropic characteristic can be an obstacle in applications as biaxial stretchable conductors. To obtain isotropic electrical conductivity, Liu et al. [23] produced CNT films by cross-stacking an even number of super-aligned CNT layers in sequence on a frame and then dipping them in ethanol to enhance the interactions between the CNTs. Because of their cross structures, the cross-stacked CNT films exhibited the same sheet resistance, approximately 405 Ω sq^{-1} for 4-layer cross-stacked films, along the directions, forming angles of 0, 30, and 45° with the *x*-axis. While the breakdown process occurred under a strain less than 4% when the films stretched along the parallel direction, the films sustained a strain of ~36% under diagonal stretching, similarly to the CNT nanomesh discussed previously. The stretchable conductor was obtained by embedding the cross-stacked CNT films in PDMS. Although the resistance of the conductor increased by 35% under a tensile strain of 30%, it increased by 15% at a strain of 28% in the second stretching process. Then, after several stretch processes, it exhibited the same trend, indicating good reversibility. A durability test confirmed the reversible electrical response. After 200 stretching/releasing cycles for a strain up to 15%, the conductor exhibited a nearly constant resistance.

Furthermore, combining this buckled configuration and cross-stacked structure can produce high-performance super-aligned CNT film-based stretchable conductors. Yu et al. [72] prepared buckled cross-stacked CNT film/PDMS conductors by cross-stacking six layers of CNT films on the 40% prestrained PDMS. The electrical performance of the resultant conductor was observed and compared with that of the buckled parallel conductor, which comprised the same number of parallel super-aligned CNT films. Although the initial resistance of the buckled cross-stacked conductor (497 Ω) was slightly larger than that of the buckled parallel conductor (430 Ω), the buckled cross-stacked one exhibited a more constant normalized resistance change. The $\Delta R/R_0$ of the cross-stacked and the parallel conductors with a buckled shape was 1.7% and 4%, respectively, under an applied strain of 40% (prestrain level). As the conductors were stretched, the super-aligned CNT arrays in the buckled cross-stacked composite were straightened until the prestrain level was reached (Fig. 4(e)). Although the CNT arrays aligned parallel to the tensile direction were fractured at a strain of 80%, which is larger than the prestrain value, the CNT arrays perpendicular to the tensile direction remained connected, as shown in Fig. 4(e). Because the CNTs were aligned along two perpendicular directions in the cross-stacked films, the buckled cross-stacked CNT film-based conductor maintained a conductive path and exhibited a far smaller resistance variation than the buckled parallel conductor.

4. CNT Yarn/Polymer Composites

If the super-aligned CNT films produced by the drawing approach pass through volatile solutions (e.g., alcohol or acetone) or are twisted, they can be converted into continuous yarns [65,73, 74]. Besides drawing from a vertically aligned CNT forest, CNT yarns can be obtained by direct spinning in the gas phase during CVD [75-77] and by the wet-spinning of CNT solutions [78-80]. The fabricated CNT yarns comprise densely aligned CNT bundles with interconnections between the individual CNTs. Their dense and compacted 1D structure contributes to their high electrical conductivity (~300 S cm^{-1}) and mechanical strength (>100 MPa) [81]. Therefore, CNT yarns show great promise for a variety of applications, such as conducting wires [82,83], tough composite fibers [79,84], and strain sensors [85,86]. However, it is difficult to apply the original CNT yarns in the straight form to stretchable electronics. CNT yarns cannot endure tensile strains greater than 10% because of the sliding among the CNTs during stretching [85,86]. Slippage and separation among the CNT bundles occur easily because of the weak van der Waals force between the bundles [87,88], resulting in a rapid resistance increase.

To resolve the limited stretchability of the CNT yarns, two main structural strategies have been introduced: creating buckled configurations and a spring-like shape. Zu et al. [89] formed a buckled structure using the prestrain method, suggesting stretchable conductors based on buckled CNT yarns. Unlike CNT films, CNT yarns cannot be bonded strongly with an elastic PDMS substrate, owing to their far smaller interfacial contact area, which may interrupt the formation of the buckling. Accordingly, to improve the interfacial bonding between the yarns and the substrate, five CNT yarns were dip-coated with a thin layer of liquid PDMS prior to being transferred onto the prestrained PDMS substrate. The release of the prestrain created a lateral kinking pattern of the CNT yarns, as depicted in Fig. 5(a). The appearance of this pattern differs significantly from the sinusoidal shape observed in buckled CNT films. This is attributed to the sliding and separation among the CNT bundles held together by the weak van der Waals force. Buckled CNT yarns can accommodate tensile strains through alternating processes of straightening and kinking without any apparent permanent fracture during multiple stretching/releasing cycles. Therefore, the buckled CNT yarn-based conductors exhibited a negligible resistance increase (~1%) under 20 stretching/releasing cycles up to the prestrain level (40%). The same research group reported a study on the long-term durability of buckled CNT yarns and stretchable conductors based on them [88]. A buckled CNT yarn was obtained by depositing CNT yarn on prestrained PDMS and then releasing it. Unlike the process for buckled pristine CNT yarn, to fabricate stretchable conductors, the five buckled CNT yarns on the PDMS were embedded within the PDMS. The resistances of the buckled pristine yarn and the stretchable conductor increased by only 1.3% and 0.2%, respectively, after 10,000 stretching/releasing cycles with a tensile strain up to 40% (prestrain level). During long-term cyclic deformation, cracks and bundle separation were observed in the kinked region of the buckled CNT yarn, as shown in Fig. 5(b), (c). On the other hand, for the stretchable conductors, the PDMS protected the CNT yarns from damage in the kinked region and interfacial debonding, yielding smaller resistance changes compared with the pristine yarn.

An alternative method for introducing elasticity into CNT yarns involves forming a spring-like shape. Fig. 5(d) shows the fabrication process for spring-like CNT yarns. The process is a modified spinning technique, which was previously reported to obtain CNT

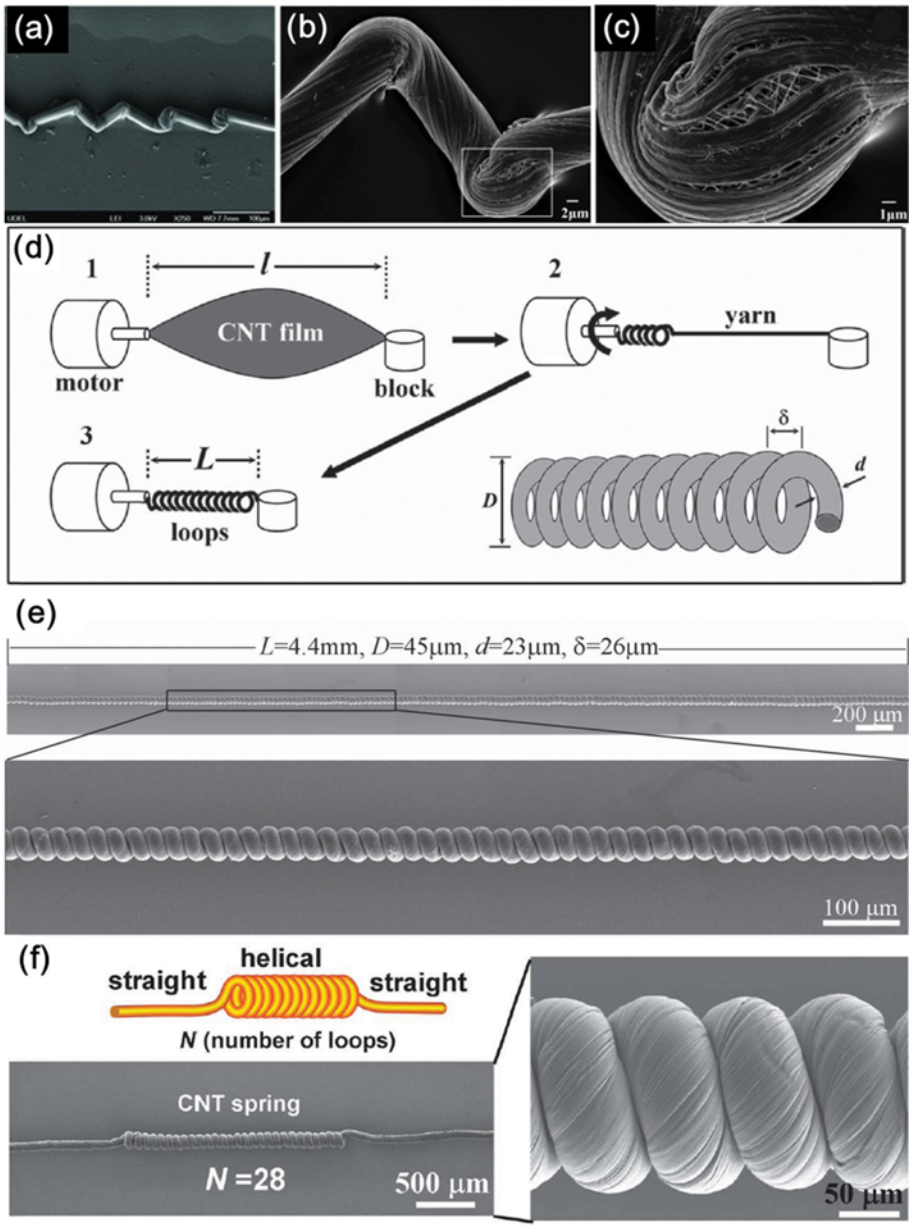

Fig. 5. (a) SEM image of one kinked CNT fiber induced by the release of the prestrained PDMS substrate. Reproduced from Ref. [89] with permission (Copyright 2012, Wiley). (b), (c) SEM images of a buckled dry-spun CNT fiber after 10,000 stretching/releasing cycles at low (b) and high (c) magnifications. Reproduced from Ref. [88] with permission (Copyright 2015, Elsevier). (d), (e) Fabrication and characterization of spring-like CNT ropes. (d) Illustration of the fabrication process: 1) a CNT film (initial length=*l*) was suspended with one end fixed on a movable block and the other end connected to a rotational motor; 2) the motor was rotated to twist-spin the CNT film into a yarn and then form helical loops by slight over-twisting, while the end block moved toward the motor because of the shortening of the yarn; 3) a CNT rope completely made of loops was produced at the final stage, with length L. The resulting spring-like structure had a yarn diameter of d, an outer-loop diameter of D, and an inter-loop distance (pitch) of δ. (e) SEM image of a 4.4-mm-long section of CNT rope consisting of highly uniform loops. Reproduced from Ref. [90] with permission (Copyright 2012, Wiley). (f) SEM images of a partial-spring CNT yarn containing 28 tightly twisted uniform loops at low and high magnifications. The inset illustrates straight-spring-straight yarn structure. Reproduced from Ref. [81] with permission (Copyright 2013, Royal Society of Chemistry).

yarns. It starts with fixing a CNT film on a rotational motor and a block. As the motor is rotated, the CNT film is converted into a yarn and then takes a spring shape with uniform and neat helical loops. Using this over-twisting approach, Shang et al. [90] reported a 4.4-mm-long spring-like CNT rope, as shown in Fig. 5(e). The resulting rope sustained tensile strains up to 285% by the opening and straightening of the loops during stretching, which is 20 times higher than the stretchability of conventional straight yarns. Owing to the spring structure, the CNT rope exhibited stable spring constants and electrical conductivity under strains up to 20% for 1,000 strain cycles. To improve the structural elasticity and electromechanical properties, a simple structural modification of a spring-

like CNT rope was conducted by the same research group [81]. Unlike their previous work on CNT ropes, a straight-helical-straight (partial-spring) CNT yarn was introduced. Fig. 5(f) shows the partial-spring CNT yarn, which consisted of a finite number of loop segments connected to the straight portions at the two sides. The partial spring-like morphology provided more uniform loops and less structural defects compared with a long yarn, with helical loops along the entire length. Consequently, the fabricated CNT yarn exhibited more stable mechanical properties under strains up to 25%, even after 1,000 stretching/releasing cycles without permanent deformation. Notably, the spring-like CNT yarns were highly stretchable without the aid of an elastic substrate, unlike the previously discussed stretchable CNT conductors. These substrate-free stretchable CNT yarns have various potential applications, such as strain sensors.

APPLICATIONS

The ultimate goal of stretchable conductors is to integrate them with other materials and structures to form stretchable devices in next-generation wearable electronics. We summarize and review here the recent progress in stretchable electronic devices based on CNTs, including strain sensors and supercapacitors.

1. Stretchable Capacitive/Resistive Strain Sensors

Stretchable strain sensors have gained increasing interest for numerous applications, including electronic skins, robotics, and biomedical procedures [91-93]. Strain sensors convert mechanical deformations into output electrical characteristics, such as capacitance or resistance. Accordingly, they can be categorized into two types: capacitive and resistive.

A capacitive strain sensor can be treated as a parallel-plate capacitor comprising two parallel conductors that act as electrodes, with a dielectric layer between the two electrodes. In the commonly used parallel-plate capacitor having an initial overlap length l_0, width w_0, and separation d_0 between the electrodes (i.e., thickness of the dielectric layer), the initial capacitance (C_0) is given as

$$C_0 = \varepsilon_0 \varepsilon_r \frac{l_0 w_o}{d_0}, \quad (1)$$

where ε_0 and ε_r represent the permittivity of vacuum and the relative permittivity of the dielectric layer, respectively. When a uniaxial tensile strain (ε) is applied to the parallel-plate capacitor, the size of the capacitor changes: the length of the electrode increases to $(1+\varepsilon)l_0$, and the width of the electrode and the distance between the electrodes decrease to $(1-v_{electrode}\varepsilon)w_0$ and $(1-v_{dielectric}\varepsilon)d_0$, respectively, where $v_{electrode}$ and $v_{dielectric}$ are the Poisson ratios of the electrodes and the dielectric layer, respectively. Assuming that the Poisson ratios are both 0.5 because the electrodes and the dielectric layer are mainly composed of polymers, the capacitance (C) is changed as follows:

$$C = \varepsilon_0 \varepsilon_r \frac{(1+\varepsilon) l_0 (1-v_{electrode}\varepsilon) w_0}{(1-v_{dielectric}\varepsilon) d_0} \cong \varepsilon_0 \varepsilon_r \frac{(1+\varepsilon) l_0 w_0}{d_0} = (1+\varepsilon) C_0. \quad (2)$$

Theoretically, the parallel-plate model exhibits a linear capacitive response to the applied tensile strain. The capacitive gauge factor is defined as the relative change in capacitance ($\Delta C = C - C_0$) divided by the mechanical strain (ε). It represents the sensitivity of the sensors, and its theoretical value is given by $(\Delta C/C_0)/\varepsilon = 1$. However, the reported gauge factors are typically less than the theoretical value of 1. For instance, the skin-like strain sensor based on spray-coated CNT films had a gauge factor of 0.4 throughout the 50% strain range [22]. It was fabricated by laminating two substrates of spray-coated CNT films/PDMS together, face-to-face, with Ecoflex as the dielectric layer. Another strain sensor, which consisted of conductive elastomeric ink (CNT-doped PDMS, CPDMS) and insulating elastomeric (plates and dielectric) architectures, had a gauge factor of 0.55 under an applied tensile strain as large as 50% [94]. CPDMS ink was prepared by dispersing CNTs in a PDMS matrix. The first step to fabricating the sensors was the formation of PDMS stamps, which were employed as the parallel plates of the capacitor by photolithography. The CPDMS ink was coated on a silicon substrate and then transferred onto the protruding parts of the PDMS stamp. After the CPDMS ink was patterned, Ecoflex—which served as insulating layer—was spin-coated onto the CPDMS-printed side of the PDMS stamp. Finally, a second CPDMS-printed stamp was laid perpendicular to the first plate.

Compared with the aforementioned sensors, highly elastic capacitive sensors capable of measuring large tensile strains above 100% with a high gauge factor of ~1 have been demonstrated. For example, Cohen et al. [60] presented a capacitive sensor with a uniform gauge factor of 0.99 throughout the entire 100% strain range. For electrodes, CNTs collected on a filtration membrane via vacuum filtration were transferred to hydrophobic regions of the silicone substrate. A higher stretchability of 150% with a gauge factor of ~1 was successfully achieved by using the two elastomer-infiltrated vertically aligned CNT-based conductors as electrodes and an intermediate elastic insulating layer [95]. Using the PDMS stamp, the vertically aligned CNT forests were patterned on the Ecoflex substrate and then infiltrated with Ecoflex to form the conductor. The capacitance increased linearly as the applied tensile strain increased. Under stepwise tensile strains up to 100% (increased by 10% for each step with a holding duration of 1 min), the gauge factors obtained from each step were almost 1 and remained stable without any irreversible degradation capacitive response. These results indicate the superior linearity and stability of the sensors. Furthermore, a strain sensor that detected extremely large strain up to 300% based on CNT films was grown by floating-catalyst CVD [96]. The CNT films were composed of random networks of CNT bundles and had a transmittance of 90% at a wavelength of 550 nm. To fabricate a parallel-plate capacitor, two layers of CNT films were laid on the two sides of a silicon elastomer. For silicone rubber, Dragon Skin was selected for its elongation, which is as large as 364%. The sensors exhibited a relatively high sensitivity with a gauge factor of 0.97.

For a resistive strain sensor, the gauge factor is defined as $(\Delta R/R_0)/\varepsilon$. Unlike capacitive strain sensors, resistive sensors offer a wide range of gauge factors: from <1 to ~70. The reported resistive gauge factors are 1 to 7 with various weights of SWCNTs in SWCNT/polymethyl methacrylate mixtures [2], 22.4 for CNT/epoxy mixtures [97], 29 for CNT-doped PDMS embedded in PDMS [98], 62 for the sandwich-like structure of spin-coated CNT films and PU-PEDOT : PSS [99], 4.5 (with pristine MWCNTs) and 178 (with

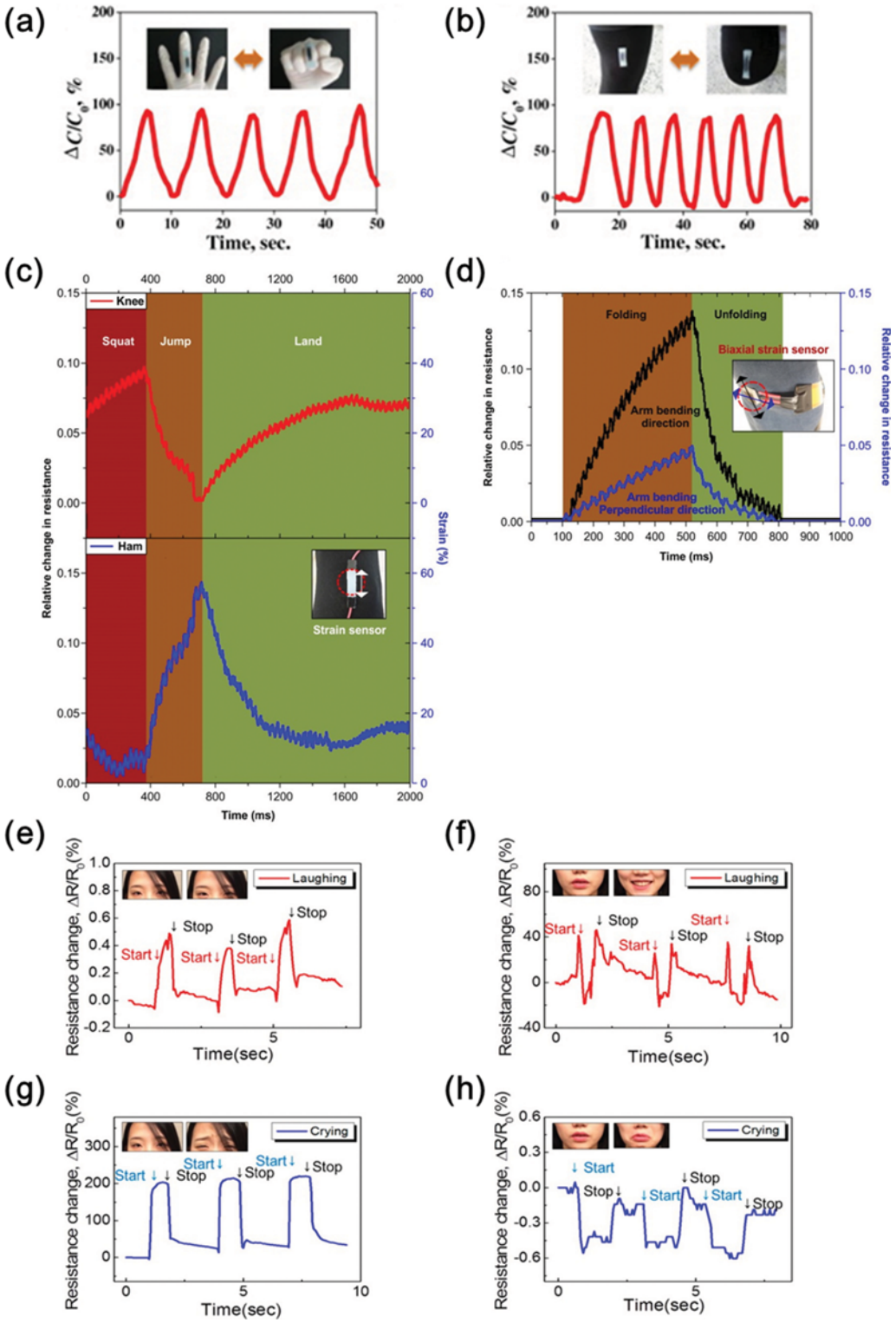

Fig. 6. (a), (b) Time-dependent relative changes in the capacitance of an elastomer-infiltrated vertically aligned CNT forest-based strain sensor under simple bending and straightening motions of the finger (a) and knee (b). (a), (b) Reproduced from Ref. [95] with permission (Copyright 2014, Elsevier). (c), (d) Wearable, extremely elastic CNT yarn-based strain sensor (substrate prestrained by 100%). (c) Time-dependent relative change in the resistance (and estimated strain) during jumping for strain sensors placed over the knee joint and hamstring muscles. (d) Time-dependent relative changes in resistance for a biaxial strain sensor placed on the elbow, with the *x*-axis parallel to the arm (black) and the *y*-axis parallel to the axis of rotation of the joint (blue). (c), (d) Reprinted from Ref. [86] with permission (Copyright 2015, American Chemical Society). (e)-(h) Time-dependent relative changes in the resistance of the sensor attached to the forehead and the skin near the mouth when the subject was laughing ((e) and (f), respectively) and crying ((g) and (h), respectively). (e)-(h) Reprinted from Ref. [99] with permission (Copyright 2015, American Chemical Society).

oxidized MWCNTs) for vacuum-filtered MWCNT dispersion on a PU membrane [100], 0.82 (0 to 40% strain range) and 0.06 (60 to 200% strain range) for CVD-grown CNT films on top of PDMS [101], 0.38 for CNT yarns embedded inside resin [85], and 0.54 (0 to 400% strain range) and 64 (400 to 960% strain range) for CNT yarns on prestrained Ecoflex [86]. Most of these sensors exhibited a high tolerance to tensile strains greater than 100%. Among them, an outstanding stretchability of 960% was achieved by dry-spun CNT yarns on prestrained (100%) Ecoflex [86]. Interestingly, for strains of 0 to 400% and 400 to 960%, the gauge factors were 0.54 and 64, respectively. At low strains, the resistance was increased by the sliding among the CNTs, and for strains greater than 400%, sliding and local disconnection between the CNTs occurred, increasing the gauge factor.

The fabricated strain sensors have been mounted on fingers, knees, and elbow joints to detect various human motions, such as grasping, bending, jumping, and running. These motions involve the extension and flexion of the joints, which cause the sensors on the joints to stretch/release and their capacitance or resistance to increase/decrease (Fig. 6(a)-(d)). Thus, the motions can be determined according to the changes in capacitance or resistance. Roh et al. [99] attached PU-PEDOT : PSS/SWCNT/PU-PEDOT : PSS-based strain sensors to facial skin to detect small strains induced by emotional expressions. The $\Delta R/R_0$ responses of a sensor attached to the forehead and skin near the mouth when a subject laughed and cried are shown in Fig. 6(e)-(h). When the person laughed

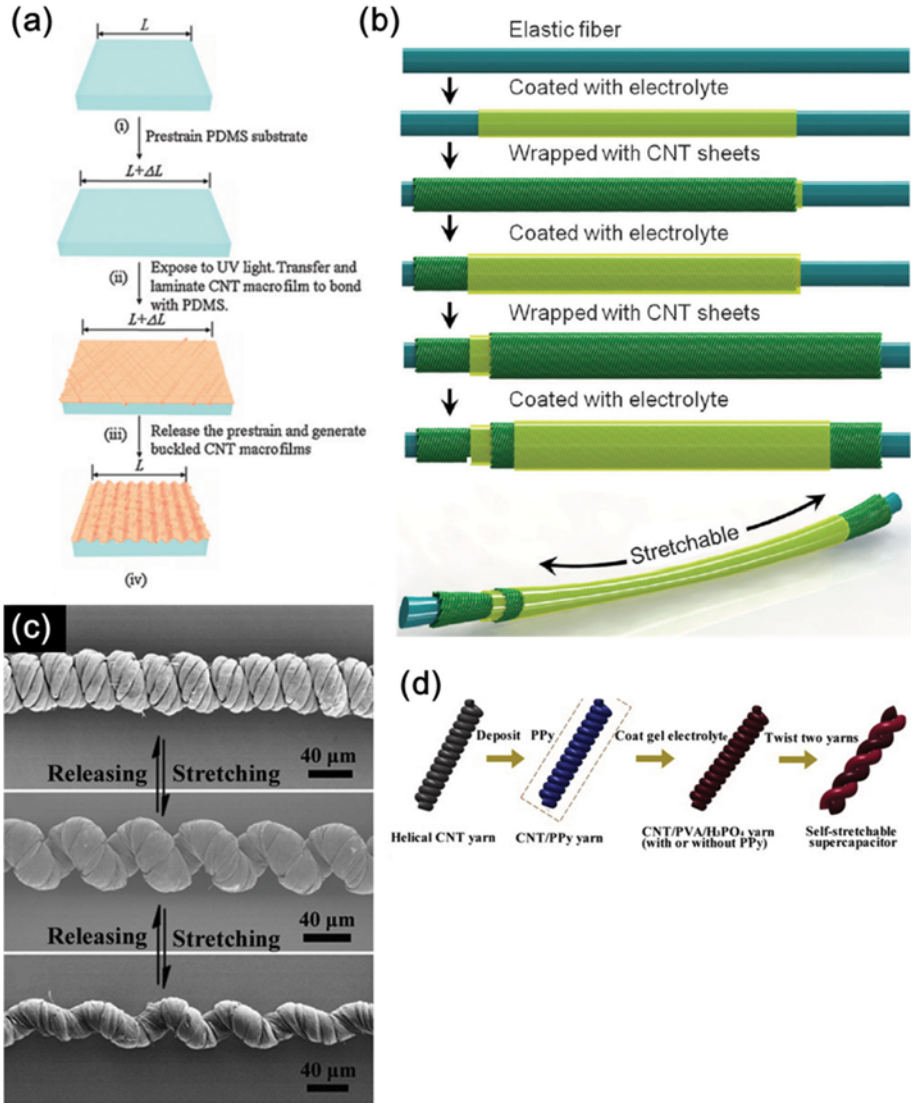

Fig. 7. (a) Fabrication steps for a buckled SWCNT film, comprising surface treatment, transfer, and the release of the prestrained PDMS substrate. Reproduced from Ref. [20] with permission (Copyright 2009, Wiley). (b) Fabrication of a highly stretchable, fiber-shaped supercapacitor with a coaxial structure. Reproduced from Ref. [112] with permission (Copyright 2013, Wiley). (c) SEM images of a spring-like CNT yarn at different strains: 0% (top), 50% (middle), and 100% (bottom). Reproduced from Ref. [115] with permission (Copyright 2014, Wiley). (d) Process whereby a helical CNT yarn (with or without polypyrrole (PPy) on the surface) was coated by a gel electrolyte and two such yarns were twisted into a fiber-shaped supercapacitor with a double-helix structure. Reproduced from Ref. [116] with permission (Copyright 2015, Elsevier).

(Fig. 6(e), (f)), the sensor on the skin near the mouth exhibited higher peak $\Delta R/R_0$ values (40%) than the sensor on the forehead (0.6%), owing to the larger movements of the muscles around the mouth. On the other hand, emotions of sadness yielded larger movements of the muscles around the forehead. Accordingly, the peak $\Delta R/R_0$ value of the sensor on the forehead was almost 200%, whereas that of the sensor on the skin near the mouth was slightly over 0% (Figs. 6(g), (h)). The differences in the response enable strain sensors to distinguish between the emotions of joy and sadness.

2. Stretchable Supercapacitors

To power stretchable electronic devices, energy-conversion and storage devices should accommodate large strains while maintaining the performance. To date, considerable effort has been directed toward the development of stretchable power-source devices such as solar cells [13], photovoltaics [102], batteries [103], and supercapacitors [104]. Among these, supercapacitors have many advantages, such as a high power and energy density, fast charge/discharge capability, long cycle life, and relatively simple design [105-107]. The maximum power of a supercapacitor is given by $P=V_i^2/4R$, where V_i is the initial voltage, and R is the equivalent series resistance [20]. Keeping the equivalent series resistance unchanged under mechanical deformation is critical for maintaining the constant power of stretchable supercapacitors.

Recently, CNT-based stretchable conductors have been employed to fabricate stretchable supercapacitors for use as electrodes. For instance, CNT/PDMS mixtures [108], CNT films on the surface of elastic substrates such as PDMS [20,107,109-111], elastic fibers [112,113] and cotton textiles [114], CNT yarns on elastomers [88], and substrate-free CNT yarns [115,116] have been reported.

Buckled CNT films were used to develop stretchable supercapacitors [20,109,110,117]. By transferring CVD-grown SWCNT films (randomly oriented SWCNTs) onto prestrained PDMS and releasing the substrate (Fig. 7(a)), buckled CNT films were formed [20]. To develop a supercapacitor, the two films were pressed together and soaked in an electrolyte. Under an applied tensile strain of 30%, the specific capacitance, energy, and power density of the stretchable supercapacitors remained nearly stable. A more stretchable supercapacitor was successfully fabricated using buckled SWCNT films with a continuous reticulate architecture, which is explained in Section 2.3 [110]. The buckled SWCNT film on PDMS, acting as an electrode, was immersed in an electrolyte solution for ~1 min. After removal and drying, two electrodes were pressed together. The resultant supercapacitors stretched under 120% strain without a significant change in performance.

By drawing the CNT film out of the vertically aligned CNT forest onto the PDMS substrate as a current collector and an active electrode, Chen et al. developed the first transparent and stretchable supercapacitors [111]. The supercapacitor, which was prepared with a cross assembly of two transparent electrodes, exhibited a specific capacitance of 7.3 F g^{-1} and a good stability when biaxially stretched with a strain up to 30%, with a transmittance of ~75% at a wavelength of 550 nm. Besides transferring onto an elastomer, drawn CNT films have been wrapped on elastic fibers to fabricate stretchable fiber-shaped supercapacitors. Yang et al. [112] produced a fiber-shaped supercapacitor with a coaxial structure by repetitively coating a thin electrolyte layer and winding a CNT film on an elastic fiber, as illustrated in Fig. 7(b). The resultant supercapacitor maintained a specific capacitance of ~18 F g^{-1} after stretching for 100 cycles at a strain of 75%. By using the prestrain approach, an extremely stretchable fiber-shaped supercapacitor that can be stretched to 350% without a significant change in the capacitive performance was demonstrated [113].

Spring-like CNT yarns have also been employed for fiber-shaped supercapacitors. Whereas buckled CNT yarns on a PDMS substrate exhibited a limited stretchability of 40% [88], CNT yarn-based fiber-shaped supercapacitors were stretched by tensile strains over 100% without a substrate. Zhang et al. [115] fabricated a stretchable supercapacitor by coating two spring-like yarns, which were prepared by over-twisting ten CNT yarns together with an electrolyte and then placing them in parallel. The supercapacitor was stretched by 100%, resulting from the elongation of the uniform coiled loops in the spring-like yarns during stretching, as shown in Fig. 7(c). Recently, a fiber-shaped supercapacitor with a double-helix structure was developed [116]. Fig. 7(d) illustrates the fabrication process. Two individual CNT yarns consisting of helical loops were coated by a thin layer of gel electrolyte and twisted together. Stretchable supercapacitors with a double-helix shape can function stably under a tensile strain up to 150%.

CONCLUDING REMARKS

We have reviewed the progress in CNT-based stretchable conductors. Early studies mainly focused on simply mixing CNTs and a polymer matrix. Then, investigations of CNT-based stretchable conductors began to use CNT films, which can be obtained by coating a CNT dispersion on an elastic substrate, performing CVD, or drawing CNTs out of a CNT forest, and CNT yarns. Stretchable structures, e.g., buckled and spring-like, were introduced to accommodate further deformations.

Despite the outstanding performance of CNT-based stretchable conductors, their absolute resistance is high compared with metal-based stretchable conductors. Therefore, CNT conductors are acceptable for voltage-driven devices but not current-driven devices. To improve the conductivity, further improvement is required regarding the materials. The large-scale and low-cost synthesis of high-quality CNTs will be beneficial for uniform performance. Furthermore, longer CNTs can reduce the number of tube-to-tube junctions. The effective metal deposition and chemical doping of CNTs can also be refined for enhanced conductivity. In addition to the conductivity, CNT-based stretchable conductors have difficulty achieving both a high stretchability and transparency. Most of the reported CNT-based stretchable conductors did not have a high transmittance above 80%. While conductors with a low transparency are used as electrodes, making them transparent can extend the applications of stretchable conductors to stretchable optoelectronics, such as displays, touch screens, solar cells, and light-emitting devices. Because of the scarcity and brittleness of indium tin oxide (ITO), which is the dominant electrode material for optical devices, several researchers have attempted to replace ITO. Therefore, to broaden the applications of stretchable CNT conductors, studies should be conducted to improve the optical transparency.

Over the past decade, tremendous research efforts have been

devoted to CNT-based stretchable conductors. With the demand for monitoring the long-term health conditions of patients, wearable sensors that continuously and simultaneously collect health information have recently received attention. Accordingly, the potential applications of stretchable conductors with regard to healthcare—including wearable sensors for health monitoring, biomedical procedures, and artificial skins for prosthetics—are expected to be an emerging field in the near future.

ACKNOWLEDGEMENTS

This research was supported by Low-dimensional Materials Genome Development by Korea Research Institute of Standards and Science (KRISS - 2016 - 16011070).

REFERENCES

1. R. F. Service, *Science*, **301**, 909 (2003).
2. I. Kang, M. J. Schulz, J. H. Kim, V. Shanov and D. Shi, *Smart Mater. Struct.*, **15**, 737 (2006).
3. C. Mattmann, F. Clemens and G. Tröster, *Sensors*, **8**, 3719 (2008).
4. K. Takei, T. Takahashi, J. C. Ho, H. Ko, A. G. Gillies, P. W. Leu, R. S. Fearing and A. Javey, *Nat. Mater.*, **9**, 821 (2010).
5. G. Schwartz, B. C.-K. Tee, J. Mei, A. L. Appleton, D. H. Kim, H. Wang and Z. Bao, *Nat. Commun.*, **4**, 1859 (2013).
6. C. Wang, D. Hwang, Z. Yu, K. Takei, J. Park, T. Chen, B. Ma and A. Javey, *Nat. Mater.*, **12**, 899 (2013).
7. T. Sekitani, H. Nakajima, H. Maeda, T. Fukushima, T. Aida, K. Hata and T. Someya, *Nat. Mater.*, **8**, 494 (2009).
8. T. Sekitani and T. Someya, *Adv. Mater.*, **22**, 2228 (2010).
9. C. Wang, W. Zheng, Z. Yue, C. O. Too and G. G. Wallace, *Adv. Mater.*, **23**, 3580 (2011).
10. S. Xu, Y. Zhang, J. Cho, J. Lee, X. Huang, L. Jia, J. A. Fan, Y. Su, J. Su, H. Zhang, H. Cheng, B. Lu, C. Yu, C. Chuang, T.-i. Kim, T. Song, K. Shigeta, S. Kang, C. Dagdeviren, I. Petrov, P. V. Braun, Y. Huang, U. Paik and J. A. Rogers, *Nat. Commun.*, **4**, 1543 (2013).
11. J. Liang, L. Li, K. Tong, Z. Ren, W. Hu, X. Niu, Y. Chen and Q. Pei, *ACS Nano*, **8**, 1590 (2014).
12. M. Amjadi, A. Pichitpajongkit, S. Lee, S. Ryu and I. Park, *ACS Nano*, **8**, 5154 (2014).
13. D. J. Lipomi, B. C. K. Tee, M. Vosgueritchian and Z. Bao, *Adv. Mater.*, **23**, 1771 (2011).
14. D. J. Lipomi, J. A. Lee, M. Vosgueritchian, B. C.-K. Tee, J. A. Bolander and Z. Bao, *Chem. Mater.*, **24**, 373 (2012).
15. P. Lee, J. Lee, H. Lee, J. Yeo, S. Hong, K. H. Nam, D. Lee, S. S. Lee and S. H. Ko, *Adv. Mater.*, **24**, 3326 (2012).
16. S.-M. Park, N.-S. Jang, S.-H. Ha, K. H. Kim, D.-W. Jeong, J. Kim, J. Lee, S. H. Kim and J.-M. Kim, *J. Mater. Chem. C*, **3**, 8241 (2015).
17. Y. Jin, S. Hwang, H. Ha, H. Park, S. W. Kang, S. Hyun, S. Jeon and S.-H. Jeong, *Adv. Electron. Mater.*, **2**, 1500302 (2016).
18. K. S. Kim, Y. Zhao, H. Jang, S. Y. Lee, J. M. Kim, K. S. Kim, J.-H. Ahn, P. Kim, J.-Y. Choi and B. H. Hong, *Nature*, **457**, 706 (2009).
19. J. Zang, S. Ryu, N. Pugno, Q. Wang, Q. Tu, M. J. Buehler and X. Zhao, *Nat. Mater.*, **12**, 321 (2013).
20. C. Yu, C. Masarapu, J. Rong, B. Wei and H. Jiang, *Adv. Mater.*, **21**, 4793 (2009).
21. Y. Zhang, C. J. Sheehan, J. Zhai, G. Zou, H. Luo, J. Xiong, Y. Zhu and Q. Jia, *Adv. Mater.*, **22**, 3027 (2010).
22. D. J. Lipomi, M. Vosgueritchian, B. C. Tee, S. L. Hellstrom, J. A. Lee, C. H. Fox and Z. Bao, *Nat. Nanotechnol.*, **6**, 788 (2011).
23. K. Liu, Y. Sun, P. Liu, X. Lin, S. Fan and K. Jiang, *Adv. Funct. Mater.*, **21**, 2721 (2011).
24. Z. Yu, X. Niu, Z. Liu and Q. Pei, *Adv. Mater.*, **23**, 3989 (2011).
25. M. Vatani, M. Vatani and J. Choi, *Appl. Phys. Lett.*, **108**, 061908 (2016).
26. A. J. Bandodkar, I. Jeerapan, J.-M. You, R. Nuñez-Flores and J. Wang, *Nano Lett.*, **16**, 721 (2016).
27. S. Duan, K. Yang, Z. Wang, M. Chen, L. Zhang, H. Zhang and C. Li, *ACS Appl. Mater. Interfaces*, **8**, 2187 (2016).
28. S. Iijima, C. Brabec, A. Maiti and J. Bernholc, *J. Chem. Phys.*, **104**, 2089 (1996).
29. T. Dürkop, S. Getty, E. Cobas and M. Fuhrer, *Nano Lett.*, **4**, 35 (2004).
30. M. Moniruzzaman and K. I. Winey, *Macromolecules*, **39**, 5194 (2006).
31. T. Cheng, Y. Zhang, W. Y. Lai and W. Huang, *Adv. Mater.*, **27**, 3349 (2015).
32. K. Kim, J. Kim, B. G. Hyun, S. Ji, S.-Y. Kim, S. Kim, B. W. An and J.-U. Park, *Nanoscale*, **7**, 14577 (2015).
33. S. Yao and Y. Zhu, *Adv. Mater.*, **27**, 1480 (2015).
34. D. McCoul, W. Hu, M. Gao, V. Mehta and Q. Pei, *Adv. Electron. Mater.*, **2**, 1500407 (2016).
35. C. F. Guo and Z. Ren, *Mater. Today*, **18**, 143 (2015).
36. S. Iijima, *Nature*, **354**, 56 (1991).
37. M.-F. Yu, O. Lourie, M. J. Dyer, K. Moloni, T. F. Kelly and R. S. Ruoff, *Science*, **287**, 637 (2000).
38. E. T. Thostenson, Z. Ren and T.-W. Chou, *Compos. Sci. Technol.*, **61**, 1899 (2001).
39. S. Shang, W. Zeng and X.-m. Tao, *J. Mater. Chem.*, **21**, 7274 (2011).
40. T. A. Kim, H. S. Kim, S. S. Lee and M. Park, *Carbon*, **50**, 444 (2012).
41. T. Sekitani, Y. Noguchi, K. Hata, T. Fukushima, T. Aida and T. Someya, *Science*, **321**, 1468 (2008).
42. M. K. Shin, J. Oh, M. Lima, M. E. Kozlov, S. J. Kim and R. H. Baughman, *Adv. Mater.*, **22**, 2663 (2010).
43. X. Ho, C. K. Cheng, J. N. Tey and J. Wei, *J. Mater. Res.*, **29**, 2965 (2014).
44. C. Zhou, J. Kong, E. Yenilmez and H. Dai, *Science*, **290**, 1552 (2000).
45. W. Zhou, J. Vavro, N. M. Nemes, J. E. Fischer, F. Borondics, K. Kamaras and D. Tanner, *Physical Review B*, **71**, 205423 (2005).
46. N. T. Selvan, S. Eshwaran, A. Das, K. Stöckelhuber, S. Wießner, P. Pötschke, G. Nando, A. Chervanyov and G. Heinrich, *Sens. Actuators A: Physical*, **239**, 102 (2016).
47. G.-X. Chen, Y. Li and H. Shimizu, *Carbon*, **45**, 2334 (2007).
48. Y. Li and H. Shimizu, *Macromolecules*, **42**, 2587 (2009).
49. K. H. Kim, M. Vural and M. F. Islam, *Adv. Mater.*, **23**, 2865 (2011).
50. L. Hu, W. Yuan, P. Brochu, G. Gruner and Q. Pei, *Appl. Phys. Lett.*, **94**, 161108 (2009).
51. X. Wang, T. Li, J. Adams and J. Yang, *J. Mater. Chem. A*, **1**, 3580 (2013).
52. M. Havel, K. Behler, G. Korneva and Y. Gogotsi, *Adv. Funct. Mater.*, **18**, 2322 (2008).
53. K. D. Behler, A. Stravato, V. Mochalin, G. Korneva, G. Yushin and Y. Gogotsi, *ACS Nano*, **3**, 363 (2009).
54. T. A. Kim, S.-S. Lee, H. Kim and M. Park, *RSC Adv.*, **2**, 10717 (2012).
55. J. W. Jo, J. W. Jung, J. U. Lee and W. H. Jo, *ACS Nano*, **4**, 5382 (2010).
56. S. Ahn, A. Choe, J. Park, H. Kim, J. G. Son, S.-S. Lee, M. Park and

H. Ko, *J. Mater. Chem. C*, **3**, 2319 (2015).
57. A. Shimoni, S. Azoubel and S. Magdassi, *Nanoscale*, **6**, 11084 (2014).
58. T. Kim, H. Song, J. Ha, S. Kim, D. Kim, S. Chung, J. Lee and Y. Hong, *Appl. Phys. Lett.*, **104**, 113103 (2014).
59. Z. Wu, Z. Chen, X. Du, J. M. Logan, J. Sippel, M. Nikolou, K. Kamaras, J. R. Reynolds, D. B. Tanner and A. F. Hebard, *Science*, **305**, 1273 (2004).
60. D. J. Cohen, D. Mitra, K. Peterson and M. M. Maharbiz, *Nano Lett.*, **12**, 1821 (2012).
61. W. Ma, L. Song, R. Yang, T. Zhang, Y. Zhao, L. Sun, Y. Ren, D. Liu, L. Liu and J. Shen, *Nano Lett.*, **7**, 2307 (2007).
62. L. Cai, J. Li, P. Luan, H. Dong, D. Zhao, Q. Zhang, X. Zhang, M. Tu, Q. Zeng and W. Zhou, *Adv. Funct. Mater.*, **22**, 5238 (2012).
63. X. Zhang, K. Jiang, C. Feng, P. Liu, L. Zhang, J. Kong, T. Zhang, Q. Li and S. Fan, *Adv. Mater.*, **18**, 1505 (2006).
64. K. Liu, Y. Sun, P. Liu, J. Wang, Q. Li, S. Fan and K. Jiang, *Nanotechnology*, **20**, 335705 (2009).
65. K. Jiang, J. Wang, Q. Li, L. Liu, C. Liu and S. Fan, *Adv. Mater.*, **23**, 1154 (2011).
66. K. Liu, Y. Sun, L. Chen, C. Feng, X. Feng, K. Jiang, Y. Zhao and S. Fan, *Nano Lett.*, **8**, 700 (2008).
67. L. Xiao, Z. Chen, C. Feng, L. Liu, Z.-Q. Bai, Y. Wang, L. Qian, Y. Zhang, Q. Li and K. Jiang, *Nano Lett.*, **8**, 4539 (2008).
68. C. Feng, K. Liu, J. S. Wu, L. Liu, J. S. Cheng, Y. Zhang, Y. Sun, Q. Li, S. Fan and K. Jiang, *Adv. Funct. Mater.*, **20**, 885 (2010).
69. Y. Zhu and F. Xu, *Adv. Mater.*, **24**, 1073 (2012).
70. F. Xu, X. Wang, Y. Zhu and Y. Zhu, *Adv. Funct. Mater.*, **22**, 1279 (2012).
71. U.-H. Shin, D.-W. Jeong, S.-H. Kim, H. W. Lee and J.-M. Kim, *ACS Appl. Mater. Interfaces*, **6**, 12909 (2014).
72. Y. Yu, S. Luo, L. Sun, Y. Wu, K. Jiang, Q. Li, J. Wang and S. Fan, *Nanoscale*, **7**, 10178 (2015).
73. M. Zhang, K. R. Atkinson and R. H. Baughman, *Science*, **306**, 1358 (2004).
74. X. Zhang, Q. Li, Y. Tu, Y. Li, J. Y. Coulter, L. Zheng, Y. Zhao, Q. Jia, D. E. Peterson and Y. Zhu, *Small*, **3**, 244 (2007).
75. Y.-L. Li, I. A. Kinloch and A. H. Windle, *Science*, **304**, 276 (2004).
76. K. Koziol, J. Vilatela, A. Moisala, M. Motta, P. Cunniff, M. Sennett and A. Windle, *Science*, **318**, 1892 (2007).
77. J. Park and K.-H. Lee, *Korean J. Chem. Eng.*, **29**, 277 (2012).
78. B. Vigolo, A. Penicaud, C. Coulon, C. Sauder, R. Pailler, C. Journet, P. Bernier and P. Poulin, *Science*, **290**, 1331 (2000).
79. A. B. Dalton, S. Collins, E. Muñoz, J. M. Razal, V. H. Ebron, J. P. Ferraris, J. N. Coleman, B. G. Kim and R. H. Baughman, *Nature*, **423**, 703 (2003).
80. L. M. Ericson, H. Fan, H. Peng, V. A. Davis, W. Zhou, J. Sulpizio, Y. Wang, R. Booker, J. Vavro and C. Guthy, *Science*, **305**, 1447 (2004).
81. Y. Shang, Y. Li, X. He, L. Zhang, Z. Li, P. Li, E. Shi, S. Wu and A. Cao, *Nanoscale*, **5**, 2403 (2013).
82. Q. Li, Y. Li, X. Zhang, S. B. Chikkannanavar, Y. Zhao, A. M. Dangelewicz, L. Zheng, S. K. Doorn, Q. Jia and D. E. Peterson, *Adv. Mater.*, **19**, 3358 (2007).
83. L. Kurzepa, A. Lekawa-Raus, J. Patmore and K. Koziol, *Adv. Funct. Mater.*, **24**, 619 (2014).
84. P. Miaudet, S. Badaire, M. Maugey, A. Derre, V. Pichot, P. Launois, P. Poulin and C. Zakri, *Nano Lett.*, **5**, 2212 (2005).
85. H. Zhao, Y. Zhang, P. D. Bradford, Q. Zhou, Q. Jia, F.-G. Yuan and Y. Zhu, *Nanotechnology*, **21**, 305502 (2010).
86. S. Ryu, P. Lee, J. B. Chou, R. Xu, R. Zhao, A. J. Hart and S.-G. Kim, *ACS Nano*, **9**, 5929 (2015).
87. M. Naraghi, T. Filleter, A. Moravsky, M. Locascio, R. O. Loutfy and H. D. Espinosa, *ACS Nano*, **4**, 6463 (2010).
88. J. Yu, L. Wang, X. Lai, S. Pei, Z. Zhuang, L. Meng, Y. Huang, Q. Li, W. Lu and J.-H. Byun, *Carbon*, **94**, 352 (2015).
89. M. Zu, Q. Li, G. Wang, J. H. Byun and T. W. Chou, *Adv. Funct. Mater.*, **23**, 789 (2013).
90. Y. Shang, X. He, Y. Li, L. Zhang, Z. Li, C. Ji, E. Shi, P. Li, K. Zhu and Q. Peng, *Adv. Mater.*, **24**, 2896 (2012).
91. F. Ilievski, A. D. Mazzeo, R. F. Shepherd, X. Chen and G. M. Whitesides, *Angew. Chem. Int. Ed.*, **50**, 1890 (2011).
92. X. Xiao, L. Yuan, J. Zhong, T. Ding, Y. Liu, Z. Cai, Y. Rong, H. Han, J. Zhou and Z. L. Wang, *Adv. Mater.*, **23**, 5440 (2011).
93. M. L. Hammock, A. Chortos, B. C. K. Tee, J. B. H. Tok and Z. Bao, *Adv. Mater.*, **25**, 5997 (2013).
94. S.-J. Woo, J.-H. Kong, D.-G. Kim and J.-M. Kim, *J. Mater. Chem. C*, **2**, 4415 (2014).
95. U.-H. Shin, D.-W. Jeong, S.-M. Park, S.-H. Kim, H. W. Lee and J.-M. Kim, *Carbon*, **80**, 396 (2014).
96. L. Cai, L. Song, P. Luan, Q. Zhang, N. Zhang, Q. Gao, D. Zhao, X. Zhang, M. Tu and F. Yang, *Sci. Rep.*, **3**, 3048 (2013).
97. N. Hu, Y. Karube, M. Arai, T. Watanabe, C. Yan, Y. Li, Y. Liu and H. Fukunaga, *Carbon*, **48**, 680 (2010).
98. N. Lu, C. Lu, S. Yang and J. Rogers, *Adv. Funct. Mater.*, **22**, 4044 (2012).
99. E. Roh, B.-U. Hwang, D. Kim, B.-Y. Kim and N.-E. Lee, *ACS Nano*, **9**, 6252 (2015).
100. P. Slobodian, P. Riha, R. Benlikaya, P. Svoboda and D. Petras, *IEEE Sens. J.*, **13**, 4045 (2013).
101. T. Yamada, Y. Hayamizu, Y. Yamamoto, Y. Yomogida, A. Izadi-Najafabadi, D. N. Futaba and K. Hata, *Nat. Nanotechnol.*, **6**, 296 (2011).
102. J. Lee, J. Wu, M. Shi, J. Yoon, S. I. Park, M. Li, Z. Liu, Y. Huang and J. A. Rogers, *Adv. Mater.*, **23**, 986 (2011).
103. A. M. Gaikwad, A. M. Zamarayeva, J. Rousseau, H. Chu, I. Derin and D. A. Steingart, *Adv. Mater.*, **24**, 5071 (2012).
104. C. Zhao, C. Wang, Z. Yue, K. Shu and G. G. Wallace, *ACS Appl. Mater. Interfaces*, **5**, 9008 (2013).
105. X. Li, J. Rong and B. Wei, *ACS Nano*, **4**, 6039 (2010).
106. X. Xiao, X. Peng, H. Jin, T. Li, C. Zhang, B. Gao, B. Hu, K. Huo and J. Zhou, *Adv. Mater.*, **25**, 5091 (2013).
107. D. Kim, G. Shin, Y. J. Kang, W. Kim and J. S. Ha, *ACS Nano*, **7**, 7975 (2013).
108. M. Yu, Y. Zhang, Y. Zeng, M. S. Balogun, K. Mai, Z. Zhang, X. Lu and Y. Tong, *Adv. Mater.*, **26**, 4724 (2014).
109. X. Li, T. Gu and B. Wei, *Nano Lett.*, **12**, 6366 (2012).
110. Z. Niu, H. Dong, B. Zhu, J. Li, H. H. Hng, W. Zhou, X. Chen and S. Xie, *Adv. Mater.*, **25**, 1058 (2013).
111. T. Chen, H. Peng, M. Durstock and L. Dai, *Sci. Rep.*, **4**, 3612 (2014).
112. Z. Yang, J. Deng, X. Chen, J. Ren and H. Peng, *Angew. Chem. Int. Ed.*, **52**, 13453 (2013).
113. T. Chen, R. Hao, H. Peng and L. Dai, *Angew. Chem. Int. Ed.*, **54**, 618 (2015).

114. L. Hu, M. Pasta, F. L. Mantia, L. Cui, S. Jeong, H. D. Deshazer, J. W. Choi, S. M. Han and Y. Cui, *Nano Lett.*, **10**, 708 (2010).
115. Y. Zhang, W. Bai, X. Cheng, J. Ren, W. Weng, P. Chen, X. Fang, Z. Zhang and H. Peng, *Angew. Chem. Int. Ed.*, **53**, 14564 (2014).
116. Y. Shang, C. Wang, X. He, J. Li, Q. Peng, E. Shi, R. Wang, S. Du, A. Cao and Y. Li, *Nano Energy*, **12**, 401 (2015).
117. J. Yu, W. Lu, S. Pei, K. Gong, L. Wang, L. Meng, Y. Huang, J. P. Smith, K. S. Booksh, Q. Li, J.-H. Byun, Y. Oh, Y. Yan and T.-W. Chou, *ACS Nano* (2016), DOI:10.1021/acsnano.6b00752.

Soo-Hwan Jeong is an associate Professor of the Department of Chemical Engineering at the Kyungpook National University (KNU). He received his B.S. degree (Yonsei University, Korea), M.S. degree (POSTECH, Korea), and Ph.D. degree (POSTECH, Korea) all in Chemical Engineering. He worked for several years at the Samsung Institute of Technology (SAIT) before joining KNU in 2005. He was a visiting professor at the University of Michigan at Ann Arbor. His research interests include various nanomaterials (carbon nanotubes, electrospun nanofibers, porous anodic alumina, and ZnO nanorods) and their applications such as sensors, transistors, stretchable conductors, and stretchable energy storage devices.